# HARP Collaboration

HARP Memo 04-001
20 May 2004
updated 31 May 2004
*http://cern.ch/dydak/wateranalysis.ps*

# Water data analysis: data reduction from beam and ITC info

G. Chelkov, A. De Min, F. Dydak, M. Gostkin, A. Guskov, Yu. Nefedov, J. Wotschack, A. Zhemchugov

CERN-HARP-CDP-2004-004
20/05/2004

**Abstract**

After recalling the motivation for the analysis of water data, the first stage of data reduction is discussed. This data reduction is based on the selection of protons using beam detector data and ITC information. The resolution of the interaction time in the target which serves as reference for time-of-flight measurement of secondaries, is determined with stable beam optics to be 77 ps, otherwise 106 ps. Cuts, their selection efficiency, event numbers, purity of the data sample after cuts, and some ITC characteristics are presented.

# 1 Motivation

The HARP experiment can possibly shed light upon the largest uncertainty in the background to the anomalous $\bar{\nu}_e$ signal observed in the LSND experiment [1], as suggested by Mills [2]. A comprehensive discussion of the physics case was presented by one of the authors (F.D.), which served as basis of a successful request to the CERN management to grant a dedicated 10-day extension of HARP data taking [3]

The LSND experiment observes a $\sim 4\sigma$ signal of $\bar{\nu}_e$-induced events above background, interpreted as an oscillation $\bar{\nu}_\mu \to \bar{\nu}_e$ with probability $(25 \pm 6 \pm 4)\times 10^{-4}$.

In LSND, neutrinos are produced by $E_{kin} = 800$ MeV protons on a target which consists largely of water, and of some iron and copper. While secondary $\pi^+$ and $\mu^+$ from their decay are essentially all stopped and produce an isotropic flux of one $\bar{\nu}_\mu$ per $\mu^+$-decay at rest, secondary $\pi^-$ are largely captured and eliminated by strong interaction before they decay; their probability of decay before capture is as small as 0.05. The grand majority of the $\mu^-$ from $\pi^-$ decay are again captured by nuclei and eliminated by weak interaction. Only 12% of captured $\mu^-$ decay and produce an isotropic $\bar{\nu}_e$ flux. Together with the assumed ratio 1:8 in the number of secondary $\pi^-$ to $\pi^+$, the net result is that the expected ratio of $\mu^-$ to $\mu^+$ decays at rest, and therefore the flux ratio of $\bar{\nu}_e$ to $\bar{\nu}_\mu$, is in the LSND experiment

$$\frac{\mu^-}{\mu^+} = \frac{1}{8} \times 0.05 \times 0.12 = 7.5 \times 10^{-4}\,.$$

This is three times smaller than the reported signal of $25\times 10^{-4}$.

The question is whether all assumptions made in the LSND background subtraction are correct within the stated systematic error. HARP can contribute to this issue with two distinct measurements:

1. the $\pi^-$ to $\pi^+$ ratio in the interaction of 1.5 GeV/$c$ protons (corresponding to $E_{kin} =$ 800 MeV protons) with water; for this measurement, data were taken with a 10% $\lambda_{abs}$ water target ('thin-water data'); is the ratio 1:8 confirmed?

2. the ratio of Michel $e^-$ to $e^+$ from the decay of stopped muons in a water target; because of the small size of the HARP water target, hardly any pion is stopped in the target and only pion decays in flight contribute; therefore, the ratio in HARP should be (1/8) $\times$ 0.12 = 0.015, since acceptance factors largely cancel); for this measurement, data were taken with a 100% $\lambda_{abs}$ water target ('thick-water data'); is the ratio of $e^-$ to $e^+$ higher than expected?

# 2 The electron signal

It is estimated that $\mathcal{O}(100)$ Michel $e^+$ can be identified in the HARP TPC from the exposure of the thick-water target which collected about $2\times 10^6$ physics events. The LSND background would amount to 1.5 $e^-$ events, whereas the LSND signal would amount to 4.5 $e^-$ events.

Michel electrons have two independent signatures: they are time-delayed according to the 2.2 $\mu$s muon lifetime at rest, and exhibit a well-known continuous momentum spectrum with an upper limit of 52 MeV/$c$. The acceptance for $e^+$ and $e^-$ in the TPC is identical and large (the maximum momentum of Michel electrons corresponds to a bending radius of 25 cm, perfectly matched to the TPC radius; Michel electrons will produce helical tracks most of which are well contained in the active TPC volume).

Abundant prompt pion background from the primary proton interaction is eliminated by a timing cut, i.e. by selecting events where the ITC hits caused by the passage of the electron and associated with a reconstructed TPC track, are delayed w.r.t. the trigger time.

# 3 Special data taking features

Since the beam intensity was carefully controlled not to exceed 5000 particles per spill, overlays in the TPC can be elimated without appreciable loss of data. Overlays from interactions before trigger time were eliminated by the usual BUSY veto which, however, was shortened from 30 $\mu$s to 15 $\mu$s. Overlays from interactions after trigger time can be eliminated by rejecting BS signals (see Section 4.1) after trigger time during the 30 $\mu$s live time of the TPC.

Because the standard 'beam trigger' was not selective enough (at +1.5 GeV/$c$ most particles are positrons (70%), then $\pi^+$ and $\mu^+$ (20%); only 10% are protons), triggering on beam protons was emphasized by a hard-wired lower limit on the time-of-flight of the beam particle.

The current of the dipole magnet was lowered by a factor of two, with a view to increasing the acceptance of low-momentum secondaries in the forward direction.

# 4 Beam particle timing with TOFA, TOFB and TDS

## 4.1 The 'time vs $z$' diagram

Three beam counters (TOFA, TOFB and TDS) with good time resolution measure the time of passage of beam particles. The algorithm developed by M. Chizhov is used to extract the most precise timing signal from the raw TDC and ADC information. The time reference for the TOFA, TOFB and TDS times is the BS counter which serves as common time reference for all time measurements in HARP.

The $z$ coordinates of these four counters are given in Table 1.

The times measured by TOFA, TOFB and TDS serve to determine the time of arrival of the beam particle at the interaction point, which in turn serves as reference for the time-of-flight of secondary particles in the RPC's and in the TOF wall.

There is strong interest in determining this reference as precisely as possible.

Conceptionally, the time of arrival of the beam particle at the interaction point is the inter-

Table 1: $z$ positions of beam counters [m].

| | |
|---|---|
| TOFA | -25.395 |
| TOFB | -4.030 |
| BS | -3.995 |
| TDS | -1.145 |

cept at the $z$ coordinate of the interaction point of a straight-line fit to the TOFA, TOFB and TDS measurements in the 'time vs $z$' diagram where the times measured by these three beam counters are plotted against their $z$ position.

Other than in the analysis of individual events where the $z$ coordinate of the interaction point will be individually determined through reconstruction and extrapolation of secondaries' tracks, we set (without loss of generality) for the purpose of this paper's discussions the interaction vertex to the position of the nominal target centre, $z = 0$.

The time of arrival of the beam particle at $z = 0$ is denoted $tz0$.

Since the BS counter is located $\sim 4$ m upstream of $z = 0$, the intercept $tz0$ depends on both the momentum and species of beam particle. Equivalently, the slope of the straight-line fit in the 'time vs $z$' diagram depends on both the momentum and species of beam particle.

With perfectly stable conditions, all straight lines from different events are expected to cross at the time of passage of the beam particle through the BS counter. Hence, deviation from the crossing point at the BS position is a measure of equipment instability, an aspect to which we will return in subsection 4.5.

The overall time resolution of TOFA, TOFB and TDS is dominated by the time resolution of the BS counter which has a large time jitter of $\sim 500$ ps. However, this poses no problem for measuring time-of-flight of secondaries since the BS time jitter cancels in their time difference to $tz0$.

The intercept $tz0$ and the slope $s$ in the 'time vs $z$' diagram are determined as follows:

$$tz0 = \frac{\sum p_i z_i^2 \sum p_i T_i - \sum p_i z_i \sum p_i z_i T_i}{\sum p_i \sum p_i z_i^2 - (\sum p_i z_i)^2} \quad (1)$$

$$\sigma_{tz0}^2 = \chi^2 \frac{\sum p_i z_i^2}{\sum p_i \sum p_i z_i^2 - (\sum p_i z_i)^2} \quad (2)$$

$$s = \frac{\sum p_i \sum p_i z_i T_i - \sum p_i z_i \sum p_i T_i}{\sum p_i \sum p_i z_i^2 - (\sum p_i z_i)^2} \quad (3)$$

$$\sigma_s^2 = \chi^2 \frac{\sum p_i}{\sum p_i \sum p_i z_i^2 - (\sum p_i z_i)^2} \ , \quad (4)$$

where $T_i$ and $z_i$ denote the measured times and $z$ positions of the three beam counters. The index $i$ runs from 1 to 3. The weights $p_i$ are given by the stochastic time resolutions $\sigma_i$ (other than the coherent BS time jitter) of the three beam counters as discussed below in subsection 4.4:

$$p_i = 1/\sigma_i^2 \ . \quad (5)$$

The $\chi^2$ in Eqs. 2 and 4 of the straight-line fit,

$$\chi^2 = \sum_{i=1}^{3} p_i (T_i - (sz_i + tz0))^2 \ , \tag{6}$$

is a measure of the linearity and therefore of the accuracy of the $z$ position of the beam counters stated in Table 1.

Besides the dominant but coherent BS time jitter, there are the following contributions to fluctuations of $tz0$ which will be discussed in turn below:

1. jumps of the average beam momentum at the same nominal momentum setting;
2. beam momentum spread;
3. intrinsic time resolution of TDS, TOFB and TOFA;
4. lack of separation between beam particle species.

While the intercept $tz0$ carries the full BS time jitter, the slope $s$ has the BS time jitter removed. Also, $s$ makes use of all available statistical information. It is therefore the most suitable variable for studies which require superior time resolution. Other suitable variables are time differences between pairs out of the TOFA, TOFB and TDS counters.

## 4.2 Jumps of average beam momentum

The intercept $tz0$ is specific for each beam momentum and for each beam particle species, but is independent of beam polarity. Unexpectedly, small adjustments turned out to be necessary to cope with minor variations of the average beam momentum across runs with the same nominal beam momentum setting of 1.5 GeV/$c$. These minor variations are conjectured to stem from beam steering manœvres.

The evidence for beam steering manœvres is shown in Fig. 1 together with Fig. 2.

Figure 1 exhibits in the run-averages of the differences TOFA–TDS and TOFA–TOFB of beam protons small jump-like deviations from the expected constancy against run number (the differences TOFA–TDS and TOFA–TOFB were chosen for their largest sensitivity to the beam proton momentum). Fig. 2 shows the run-averages of the horizontal and vertical angles of the beam proton at the target position. The correlation of the occurrence of jumps is obvious and supports the conjecture of beam optics changes, rather than instabilities of the beam counters.

Accordingly, the data are subdivided into groups of run numbers which are considered to have stable beam optics. For each group, the averages of TOFA, TOFB, and TDS are given in Table 2, their straight-line intercept $tz0$, their slope $s$, the $\chi^2$ of the fit, and the proton momentum.

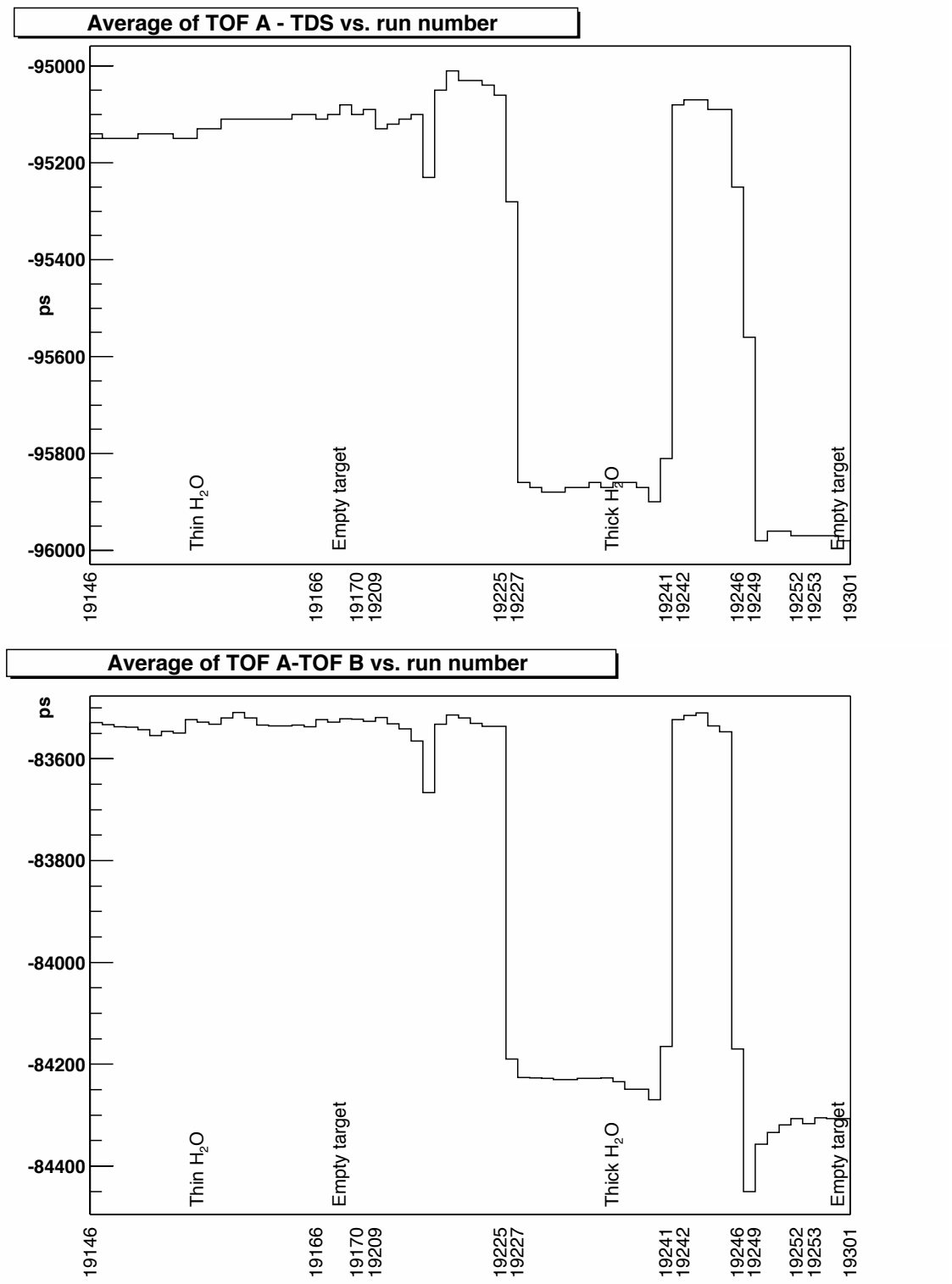


Figure 1: Average of TOFA–TDS (top) and TOFA–TOFB (bottom) of beam protons versus run number. Notice that the vertical scale has zero suppressed.

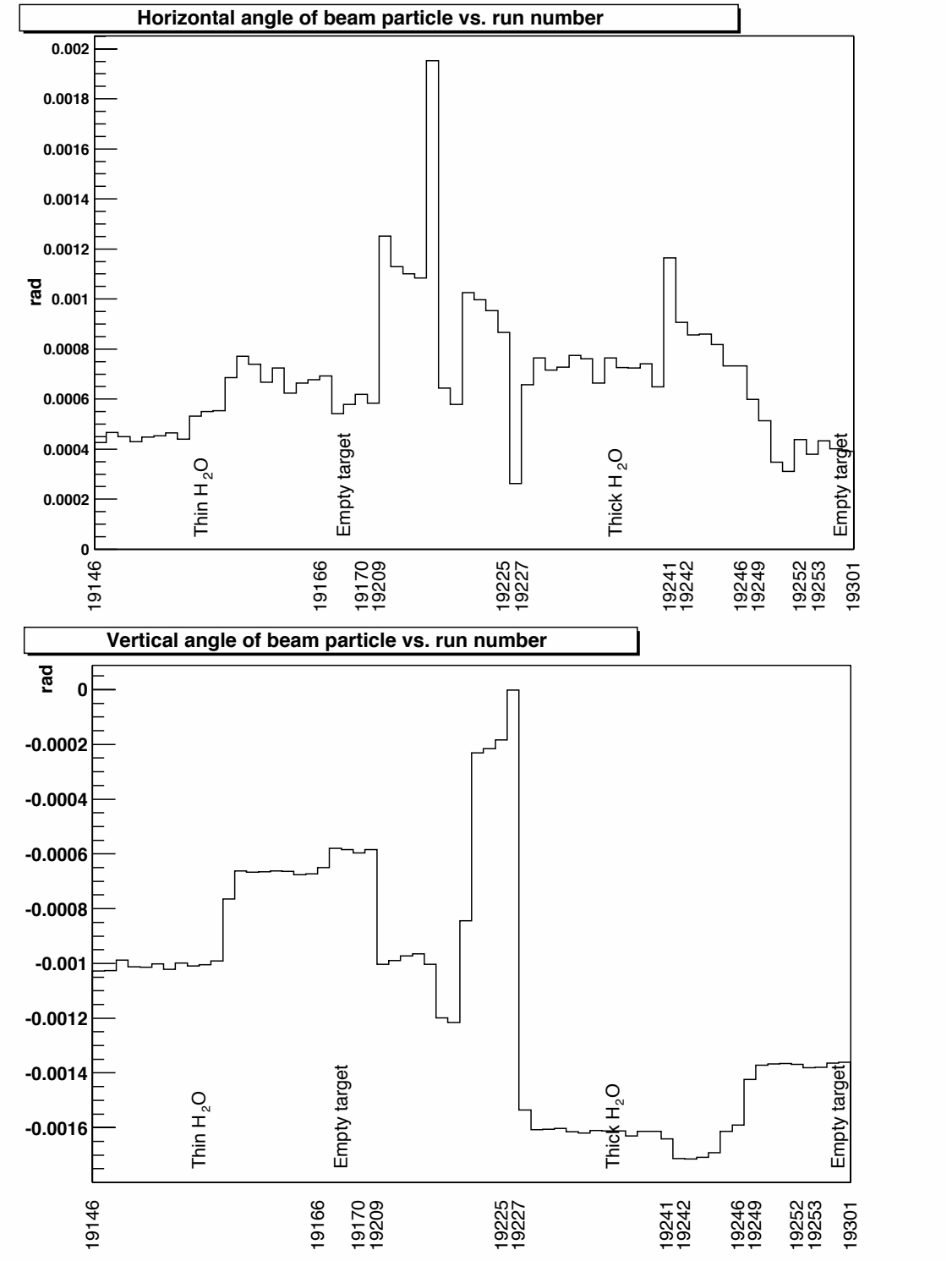


Figure 2: Horizontal (top) and vertical (bottom) angle of beam protons before the target.

Table 2: Time averages [ps] of TOFA, TOFB, and TDS of beam protons, their straight-line intercepts $tz0$, their slope $s$, the $\chi^2$ of the fit, and the proton momentum. The data are given separately for groups of run numbers which are considered to have stable beam optics.

| From | To | ⟨TOFA⟩ | ⟨TOFB⟩ | ⟨TDS⟩ | intercept | slope | $\chi^2$ | momentum |
|---|---|---|---|---|---|---|---|---|
| 19146 | 19166 | -119212 | -35676 | -24088 | -19745 | 3.9171 | 2.315 | 1.520 |
| 19209 | 19225 | -119400 | -35858 | -24334 | -19963 | 3.9160 | 1.440 | 1.521 |
| 19227 | 19241 | -120135 | -35886 | -24262 | -19854 | 3.9494 | 1.486 | 1.476 |
| 19242 | 19246 | -119430 | -35900 | -24353 | -19993 | 3.9160 | 1.747 | 1.521 |
| 12249 | 19252 | -120219 | -35868 | -24240 | -19823 | 3.9537 | 1.377 | 1.471 |

We notice from the entries in Table 2 that the average times of the TOFB counter is only stable within $\sim 200$ ps. Since the TOFB counter is very close to the BS counter, we would *a priori* expect constancy of the TOFB time. The most likely explanation of this drift is a small instability of the response of the BS counter which is at this level not unexpected.

We note that shifts of the BS response have no bearing on the precision of time-of-flight measurements.

Figure 3 shows the straight-line fits in the 'time vs $z$' diagram for the five groups of data listed in Table 2.

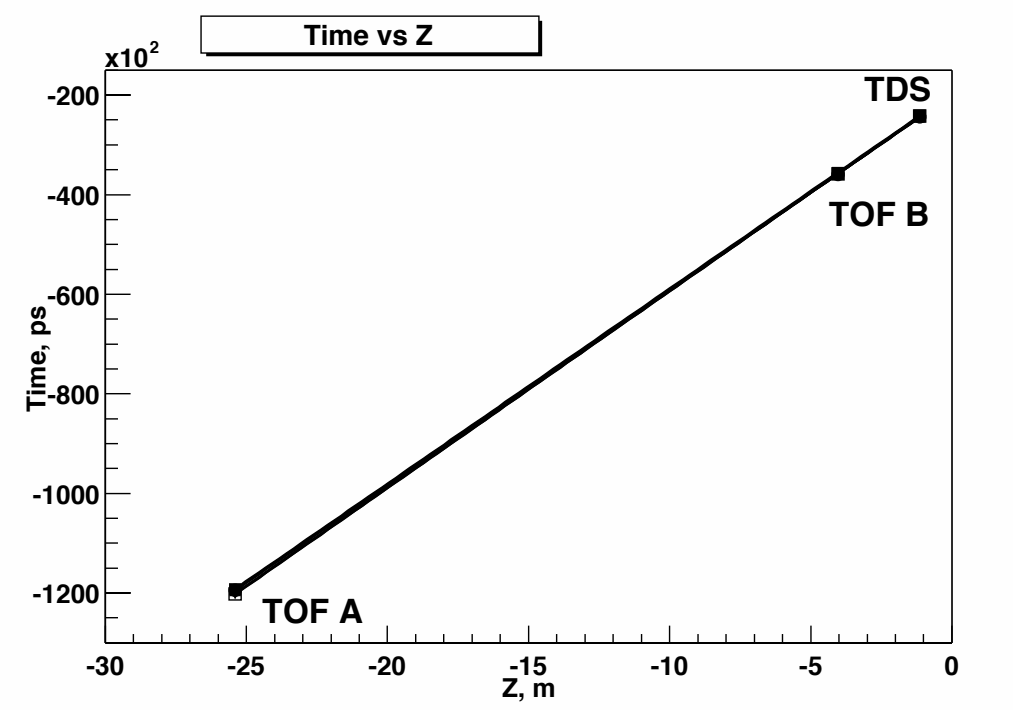


Figure 3: Straight-line fits in the 'time vs $z$' diagram for the five groups of data listed in Table 2.

## 4.3 Beam momentum spread

The beam momentum has a finite spread around its average value which for the optics of the T9 beam is expected to be about 1%. This spread leads to a stochastic fluctuation of the slope $s$ and the intercept $tz0$, and contributes through the latter to the accuracy of time-of-flight measurement.

Table 3 assesses the impact of a 1% beam momentum spread on $tz0$, for various beam momenta and beam particle species. From Table 3 it appears that in comparison to the

Table 3: Fluctuation of $tz0$ in ns for various beam momenta and beam particle species.

| Beam momentum (GeV/$c$) | $\sigma_{t_{\mathrm{Proton}}}$ | $\sigma_{t_{\mathrm{Pion}}}$ | $\sigma_{t_{\mathrm{Electron}}}$ |
|---|---|---|---|
| 1.5 | 0.044 | 0.001 | 0.000 |
| 3.0 | 0.012 | 0.000 | 0.000 |
| 5.0 | 0.005 | 0.000 | 0.000 |
| 8.0 | 0.002 | 0.000 | 0.000 |
| 10.0 | 0.001 | 0.000 | 0.000 |
| 12.0 | 0.001 | 0.000 | 0.000 |
| 15.0 | 0.001 | 0.000 | 0.000 |

fluctuation of the intercept $tz0$ from the intrinsic time resolution of the beam counters ($\sim$ 100 ps, see Section 4.4), only 1.5 GeV/$c$ protons with a stochastic fluctuation of 44 ps due to a 1% beam momentum spread merit further attention.

In the subsequent Section 4.4, after the discussion of the intrinsic time resolutions, the actual momentum spread of protons at the 1.5 GeV/$c$ momentum setting will be determined.

## 4.4 Intrinsic time resolutions of TOFA, TOFB and TDS

For a well separated beam particle species, the stochastic time resolution of the differences TOFA–TDS, TOFA–TOFB and TOFB–TDS is determined from (i) the intrinsic time resolutions of the TOFA, TOFB and TDS counters, and (ii) the fluctuations caused by the beam momentum spread.

With $\sigma_p$ denoting the relative beam momentum spread, the resulting fluctuation of the time difference between beam counters $i$ and $j$ is for beam protons

$$\sigma_{\Delta t_{i,j}} = \frac{m_{\mathrm{P}}^2}{pE_{\mathrm{P}}} \frac{1}{c} \sigma_p (z_i - z_j) \; , \tag{7}$$

where $m_{\mathrm{P}}$ denotes the proton mass, $E_{\mathrm{P}}$ the proton energy, $p$ the beam momentum, $c$ the speed of light, and $z_i - z_j$ the flight path between beam counters $i$ and $j$.

Table 4 gives the results for the three possible time differences. This system of three equations for four unknowns is under-determined. Therefore, from -12 GeV/$c$ beam pion data which are insensitive to time differences from beam momentum spread, the time differences given in

Table 4: Time differences of beam counters in a 1.5 GeV/$c$ proton beam.

| Difference | Squared theor. resolution | Exp. resolution [ps] |
|---|---|---|
| TOFA–TDS | $\sigma^2_{\mathrm{TOFA}} + \sigma^2_{\mathrm{TDS}} + \sigma^2_{\Delta t_{\mathrm{TOFA,TDS}}}$ | 268.4 |
| TOFA–TOFB | $\sigma^2_{\mathrm{TOFA}} + \sigma^2_{\mathrm{TOFB}} + \sigma^2_{\Delta t_{\mathrm{TOFA,TOFB}}}$ | 249.3 |
| TOFB–TDS | $\sigma^2_{\mathrm{TOFB}} + \sigma^2_{\mathrm{TDS}} + \sigma^2_{\Delta t_{\mathrm{TOFB,TDS}}}$ | 189.1 |

Table 5 have been measured, which permit the determination of the intrinsic time resolutions of TOFA, TOFB and TDS. Figures 4, 5 and 6 show the three analogous time differences for

Table 5: Measured resolutions of the time differences between beam counters in a -12 GeV/$c$ pion beam, and the resulting individual time resolutions of the beam counters.

| | Resolution [ps] | | Resolution [ps] |
|---|---|---|---|
| TOFA–TDS | 170.9 | TOFA | 101 |
| TOFA–TOFB | 165.0 | TOFB | 130 |
| TOFB–TDS | 189.5 | TDS | 138 |

the case of 1.5 GeV/$c$ protons. The whole statistics of the water data are shown in these plots, after adjustments for the jumps in the average beam momentum. With the intrinsic time resolutions of the three beam counters given in Table 5, we obtain from Eq. 7 a beam momentum spread of

$$\frac{\Delta p}{p} \sim 0.008 \; .$$

This value is consistent with what is expected from the T9 beam optics.

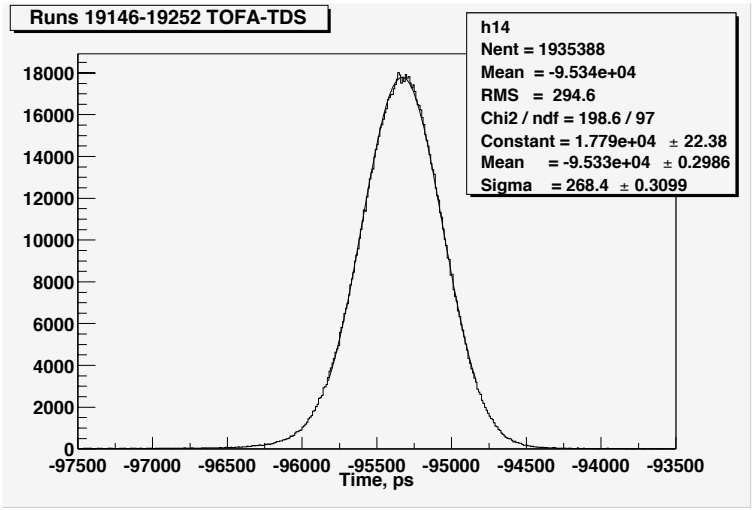


Figure 4: The difference TOFA–TDS after correction for beam steering changes, for all events with TOFA, TOFB and TDS hits.

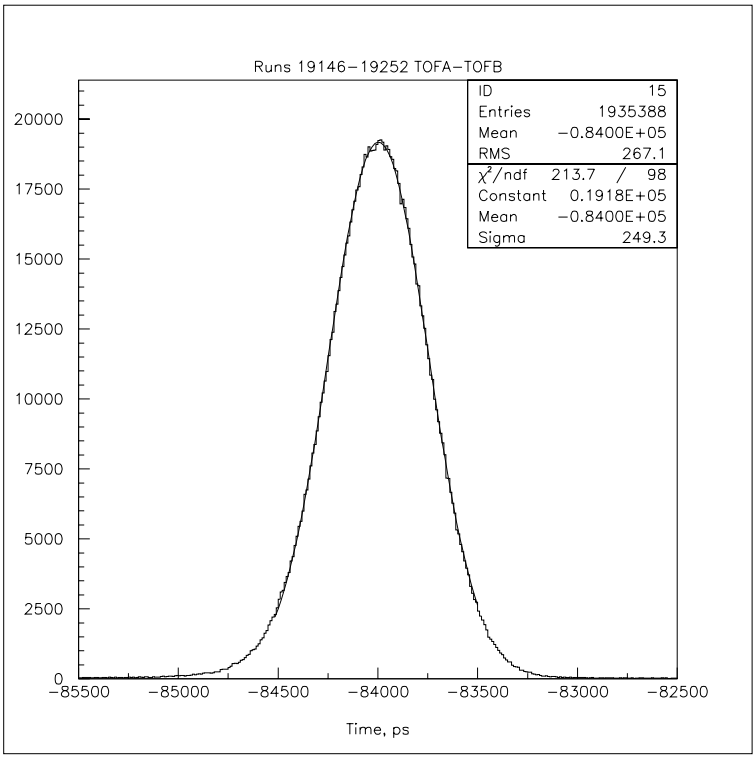


Figure 5: The difference TOFA–TOFB after correction for beam steering changes, for all events with TOFA, TOFB and TDS hits.

We conclude from Table 3 that a beam momentum spread of 0.8% leads to a fluctuation of the intercept $tz0$ of 35 ps. This is to be compared to the fluctution from the intrinsic time resolution which is calculated from Eq. 2 to be 106 ps, where the $z$ positions given in Table 1 and the time resolutions given in Table 5 are used.

## 4.5 Obtaining the best time-of-flight precision

For data taken with stable beam optics, a better statistical precision of the intercept $tz0$ can be obtained for an individual event, if a constant average slope $\langle s \rangle$ is used *in lieu* of an event-specific slope. With an average slope $\langle s \rangle$, the statistical fluctuation of the intercept $tz0$ from the intrinsic time resolution of the three beam counters will decrease from 106 ps to 69 ps.

Neither the coherent BS time jitter nor small shifts with time of the BS timing has a bearing on this consideration. But the spread of beam momentum and a lack of separation between beam particle species has. This is because both effects cause not a stochastic fluctuation of each beam counter, but a fluctuation which is correlated across the three beam counters.

If a constant slope is used but there is a variation of the slope due to momentum spread, or lack of separation between beam particle species, this would effectively lead to a fluctuation of the intercept $tz0$, which is absent if one uses an event-specific slope. One would gain in

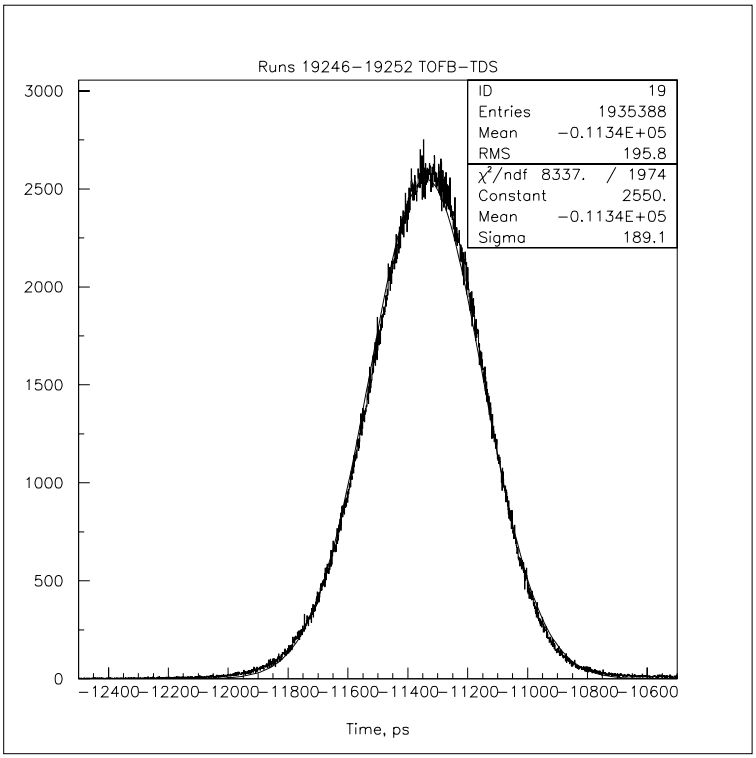


Figure 6: The difference TOFB–TDS after correction for beam steering changes, for all events with TOFA, TOFB and TDS hits.

precision only if the condition

$$\sigma_{\rm ms}^2 + 69^2 < 106^2 \tag{8}$$

holds, where $\sigma_{\rm ms}^2$ is the apparent fluctuation caused by beam momentum spread and/or lack of separation of beam particle species when employing an average slope $\langle s \rangle$. Equation 8 holds when $\sigma_{\rm ms}^2$ is smaller than 80 ps.

Given the above-determined momentum spread of 0.8% in the 1.5 GeV/$c$ beam, we conclude that **for 1.5 GeV/$c$ protons, the use of an average slope $\langle s \rangle$ for groups of data with stable conditions,** *in lieu* **of an event-specific slope $s$, permits superior precision in the intercept $tz0$.**

With stable beam optics, i.e. by use of a constant average slope, the time resolution of the intercept $tz0$ is thus $\sqrt{69^2 + 35^2} = 77$ ps. If an event-specific slope has to be used, the time resolution is 106 ps.

At the 1.5 GeV/$c$ beam momentum of the water data, protons and pions are so well separated by beam counter time-of-flight that there is no confusion. However, at higher momenta the time-of-flight distributions start to overlap. The apparent difference in the intercept $tz0$ when using a constant average slope is given in Table 6 for various beam momenta, for protons and pions as beam particles. The conclusion is that the use of a constant average slope $\langle s \rangle$ causes no problems for beam momenta up to 3 GeV/$c$, because protons and pions are well separated. At beam momenta of 10 GeV/$c$ and above, the effect is small enough not to deteriorate appreciably the resolution of the intercept $tz0$. But there is a problem

Table 6: Apparent difference $\Delta tz0$ of the intercepts for various beam momenta, between protons and pions.

| Beam momentum [GeV/$c$] | $\Delta tz0$ [ns] |
|---|---|
| 1.5 | 2.335 |
| 3.0 | 0.622 |
| 5.0 | 0.227 |
| 8.0 | 0.089 |
| 10.0 | 0.057 |
| 12.0 | 0.040 |
| 15.0 | 0.025 |

for beam momenta between 3 and 10 GeV/$c$, so that for these beam momenta the use of an event-specific slope is warranted.

# 5 Cuts for selecting good beam protons

We give below the set of cuts chosen with a view to selecting as many good beam protons as possible.

**Cut 1.1: One and only one hit in TOFA and TOFB**

Figure 7 shows the time difference, after correction for beam steering changes, between the single hits in TOFA and TOFB, for all events which pass Cut 1.1.

**Cut 1.2: The time difference TOFA–TOFB is between -77 ns and -89 ns**

The average value of this time difference is -84.1 ns. The surviving proton sample has 100% purity.

**Cut 1.3: In the three planes with vertical wires of the three small MWPC's, and independently in the three planes of horizontal wires, not less than one and not more than two hits are required in each plane; the selected hits are those with a straight-line fit with the smallest $\chi^2$, in both the $x$ and $y$ projections; the smallest $\chi^2$ must be below 10.**

Figure 8 shows the distribution of the smallest $\chi^2$ (the spike at $\chi^2 = 21$ is an artifical accumulation of rejected cases).

Cut 1.3 is necessary because the trajectory of the incoming proton must be known to define the interaction vertex and permit a cut on the fiducial water-target volume.

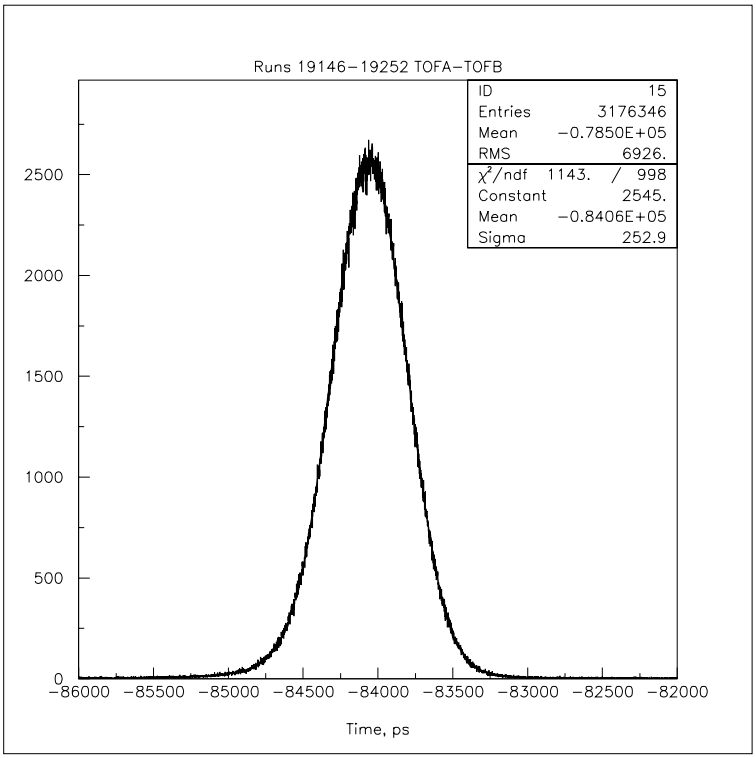


Figure 7: The difference TOFA–TOFB after correction for beam steering changes, for all events with one TOFA hit and one TOFB hit.

# 6 In-time hits in the ITC counters

The next cut is the requirement of hits in the ITC counter at trigger time (in-time hits), which are consistent with a physical track from the target into the active TPC volume. Since the efficiency of the ITC layers is considerably below 100%, the following requirement is made:

**Cut 2.1: At least one hit in any two of the three layers of ITC counters; the time of both hits must coincide within 10 ns with the trigger time; if the two hits are in the two inner ITC layers, they must be geometrically correlated.**

The geometrical correlation requires that a hit in a channel of layer 1 is accompanied by a hit in the channel of layer 2 with the same azimuthal coordinate, or in its left or right neighbour channels (this choice is not only made to cope with the track bending in the solenoidal magnetic field, but also with construction inadequacies of the ITC, see below).

The study of in-time hits permits an approximate estimate of the average efficiency of the three ITC layers. For example, the average efficiency of layer three is determined from the comparison of the number of events with one and only one in-time hit both in layers 1 and 2, with the number of events when in addition one or two in-time hits in layer 3 are requested (layer 3 is a double-layer). The results for the average efficiencies are given in Table 7. While the loss of events due to the less than perfect efficiency of the ITC layers is negligible for in-time tracks (because of the average charged multiplicity of $\sim 3$), it is at the 10% level

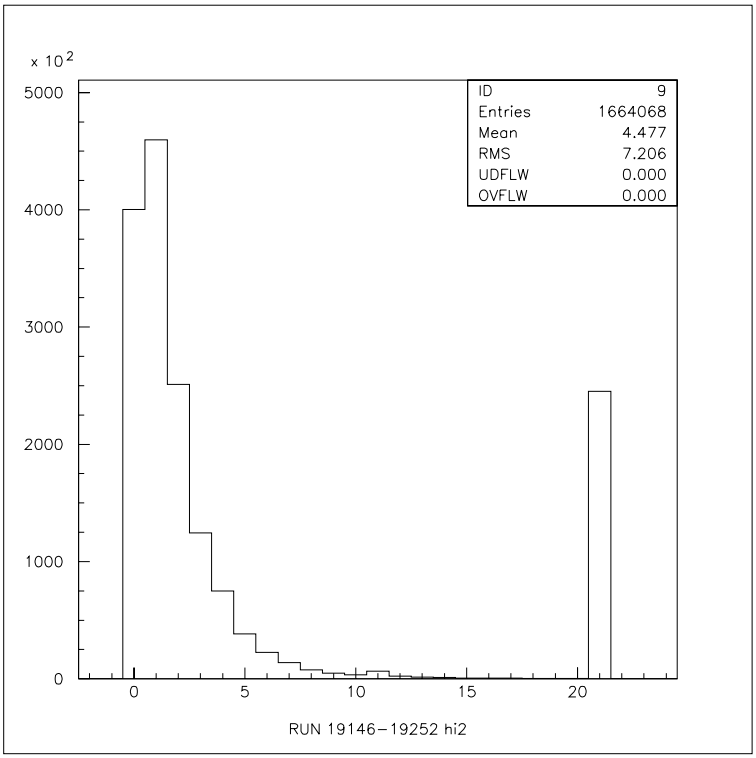


Figure 8: $\chi^2$ distribution of MWPC straight-line fits.

from the necessary requirement of a delayed single track.

Table 7: The average efficiency of the three ITC layers.

| Layer number | Efficiency |
|---|---|
| 1 | .81 |
| 2 | .77 |
| 3 | .80 |

Figure 9 shows the ITC hit statistics as a function of the ITC channel number. The third layer is more noisy than the two inner layers. Channel 16 sticks out as particularly noisy.

Figures 10 shows the channel number of in-time hits (one and only one) of ITC layer 1 (channels 0 to 7) against the channel number of in-time hits (one and only one) of ITC layer 2 (channels 8 to 15). The good news are that there is very little uncorrelated noise. The bad news are: (i) either channels 0 and 1 in the first layer, or channels 8 and 9 in the second layer are interchanged; (ii) in either channels 6 and 7 in the first layer, or in channels 14 and 15 of the second layer, nearly half of the fibres of one channel are wrongly connected to the other channel (this is corroborated by inspection of Fig. 11 which shows the channel counts in layers 1 and 2, which clearly exhibit a lower efficiency in channels 6 and 7, and 14 and 15, respectively); and (iii) layers 1 and 2 have a small azimuthal misalignment with respect to each other. These deficiencies as well as the less than perfect efficiency of the ITC will have

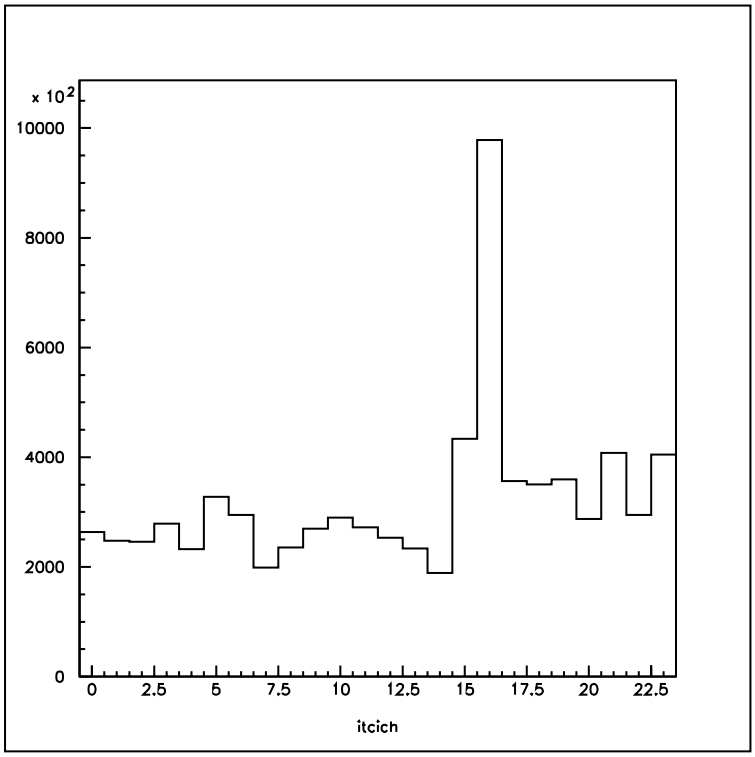


Figure 9: Frequency of ITC hits as a function of the ITC channel number (layer 1: channels 0 to 7; layer 2: channels 8 to 15; layer 3: channels 16 to 23).

to be carefully considered, should one day a serious measurement of absolute cross-section be intended.

From this point onwards, the data reduction of thick- and thin-water data splits into two different analysis paths. The cut below is applied to thick-water data only.

# 7 Delayed hits in the ITC counters

A specific feature of the electron analysis is the requirement of hits in the ITC counters which are consistent with the existence of a second, delayed, physical track from the target region into the active TPC volume:

**Cut 3.1: At least one hit in any two of the three layers of ITC counters, with a time delayed by at least 200 ns w.r.t. the trigger time; the time of the two hits must coincide within 10 ns; if the two hits are in the two inner ITC layers, they must be geometrically correlated; no BS hit must be closer than 20 ns to the average of the time of the two ITC hits.**

The choice of 200 ns has two motivations. The first is to require a minimum distance in $z$ between the vertex of the primary track, and the closest distance of approach of the second track to the z axis (200 ns correspond to 1 cm), to ensure that the two tracks do not originate from the same vertex.

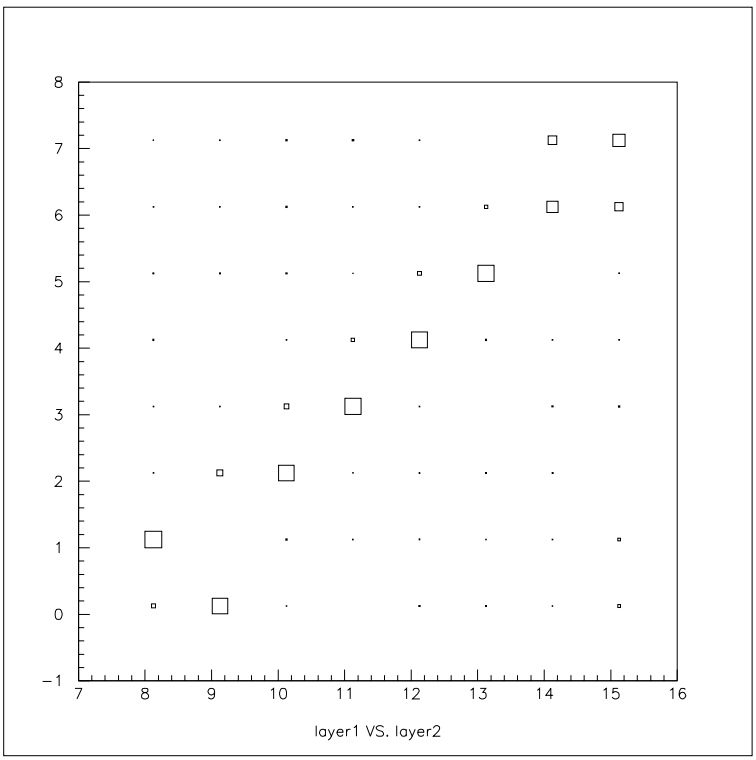


Figure 10: Correlation of the number of in-time ITC hits between the channels of layer 1 (0 to 7) and the channels of layer 2 (8 to 15); data from run 19249.

The second motivation is to reduce the large background of ITC hits from afterpulsing in the PMT's due to feedback from ionized atoms and molecules. To illustrate the latter phenomenon which is, not unexpectedly, irregular across different PMT's, Fig. 12 shows the time spectrum of afterpulses for times larger than 30 ns after the trigger time, for one of the ITC PMT's.

At this point of the reduction of thick-water data, the background to the Michel electron signal is expected to consist of

1. fake tracks due to chance coincidences of random noise of the ITC PMT's (with a flat time distribution);
2. fake tracks due to coincidences of afterpulse hits of the ITC PMT's (with an irregular time distribution);
3. cosmic ray tracks (with an exponentially falling but *de facto* flat time distribution).

Figure 13 shows the time delay w.r.t. the trigger signal, of the first accepted delayed concidence of hits in any two ITC layers.

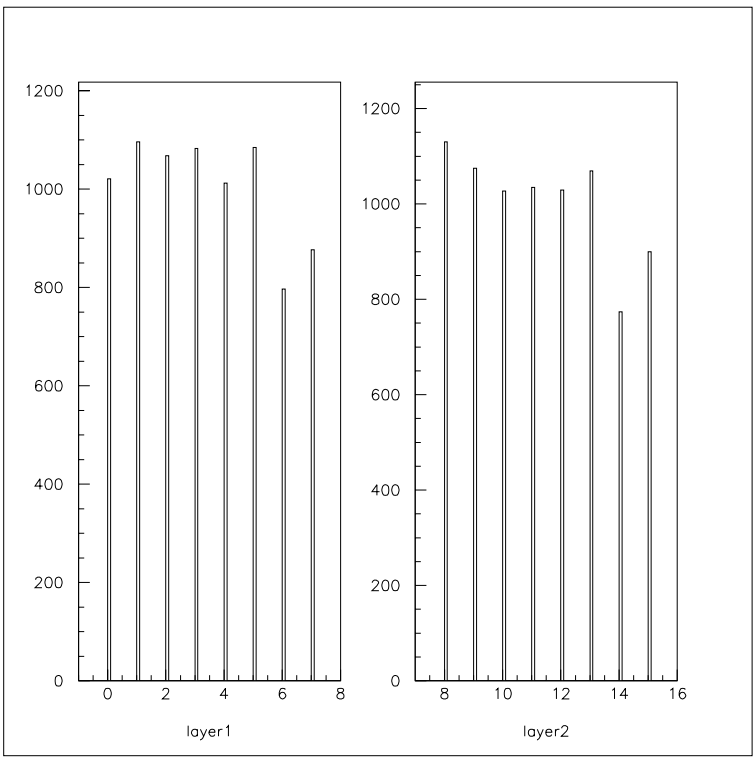


Figure 11: Number of ITC hits for the channels of layer 1 (left) and layer 2 (right); data from run 19249.

# 8 Summary of event numbers

Table 8 gives the number of events before cuts, and after each cut, for both the thin-water and thick-water data samples. The term 'before cuts' refers to physics events minus events that had readout errors.

A preliminary account of this data reduction was given by Gostkin in a presentation of preliminary results to the Collaboration [4]. The final number of events after cuts presented here is considerably higher because great care was taken to optimize the software, with a view to avoiding unnecessary loss of data.

Of particular interest is the reduction of the number of events in the thick-water sample: the reduction factor is 15.5 .

# 9 Distribution of protons on the water targets

Figure 14 shows a scatterplot of the $x$ and $y$ coordinates of beam protons at $z = 0$ for the thin- and thick-water targets, for the event samples after cuts 2.1 and 3.1, respectively. The $x$ and $y$ coordinates are independently reconstructed from straight-line fits to hits in three planes of the small MWPC.

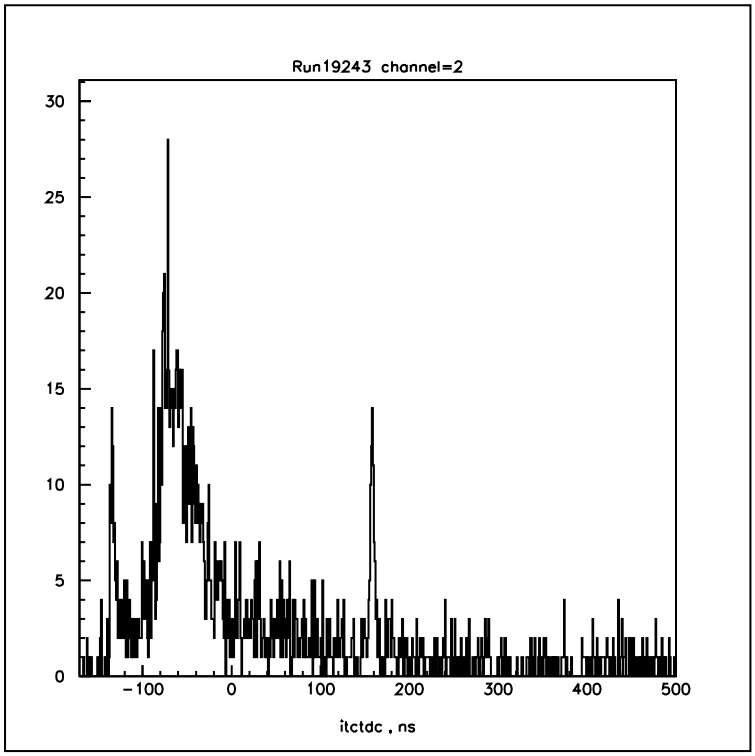


Figure 12: Time spectrum of afterpulses more than 30 ns after the trigger time, for one of the ITC PMT's.

Table 8: Number of events as a function of cuts for thin- and thick-water data.

| | **Thin-water data** | **Thick-water data** | **Thin-water background** | **Thick-water background** |
|---|---|---|---|---|
| | Number of events | Number of events | Number of events | Number of events |
| Before cuts | 1523739 | 2081949 | 227360 | 296328 |
| After Cut 1.1 | 1323406 | 1852940 | 200198 | 259630 |
| After Cut 1.2 | 278787 | 1385281 | 30632 | 196494 |
| After Cut 1.3 | 227296 | 1172421 | 24071 | 164945 |
| After Cut 2.1 | 49144 | 604532 | 1299 | 3407 |
| After Cut 3.1 | — | 134319 | — | 795 |

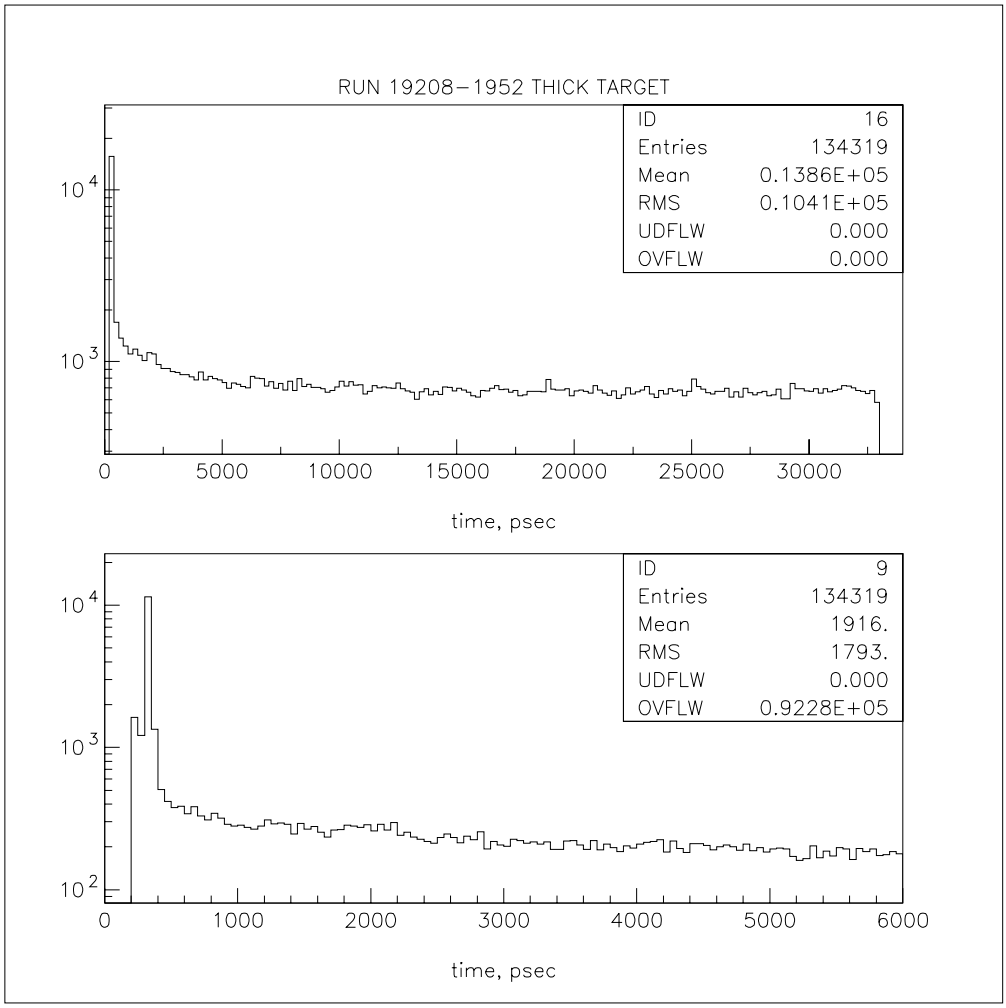


Figure 13: Time delay of delayed ITC coincidences with respect to the trigger time; the lower plot shows the same selection as the upper plot but emphasizes the time window of the signal of delayed electrons.

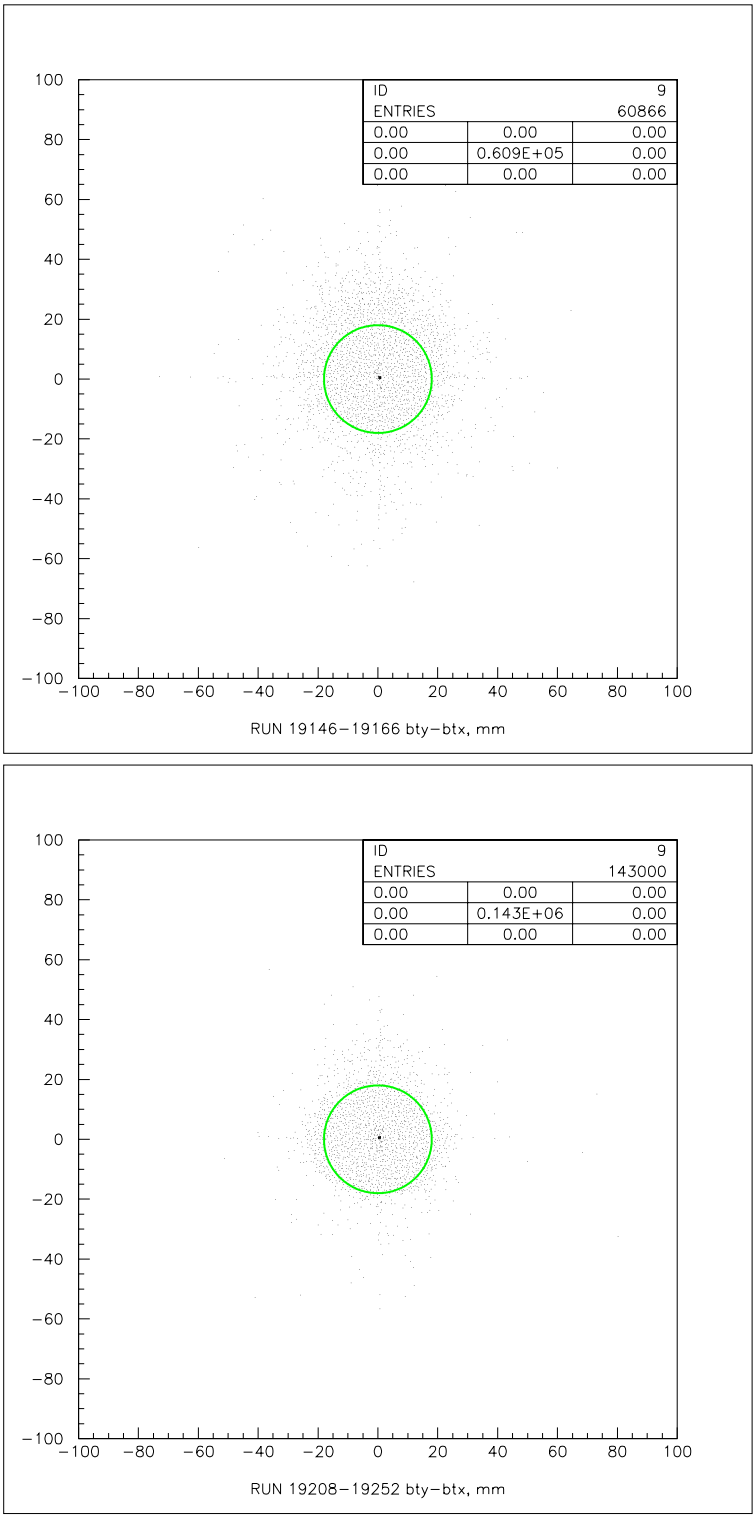


Figure 14: Scatterplot of the $x$ and $y$ coordinates of beam protons at $z = 0$ for the thin-water (top) and thick-water (bottom) targets; the circles show the outer circumference of the water volumes.

## Acknowledgement

We wish to thank C. Wiebusch for his contributions in the early stage of the water-data reduction from beam and ITC info.

# References

[1] A. Aguilar *et al.* (LSND collaboration), Phys. Rev. **64** (2001) 112007.

[2] Suggestion made by G. Mills (LANL) on 13.9.2002.

[3] F. Dydak, Memorandum 'A contribution to the LSND puzzle?' (23.9.2002), *http://cern.ch/dydak/LSNDriddle.ps*

[4] A. De Min *et al.*, Water data analysis: Data reduction from beam and ITC info, presented by M. Gostkin on 17.2.2004 in a HARP Collaboration Meeting.